Dynamic Modeling and Real-Time Simulation of a Ship Hybrid Power System Using a Mixed-Modeling Approach

Pramod Ghimire*†, Namireddy Praveen Reddy*, Mehdi Karabalaye Zadeh*, Eilif Pedersen*, and Jarle Thorstensen†

*Department of Marine Technology, Norwegian University of Science and Technology, Trondheim, Norway
†Kongsberg Digital AS, Horten, Norway
Email: pramod.ghimire@ntnu.no

Abstract—The electrification of a ship power-train is growing at a fast pace to improve efficiency and reduce emissions. The implementation of new technologies requires test and validation using various modeling approaches. However, many of the existing models of the ship hybrid power system are too complicated and demand high computational requirements, which make them inappropriate for the real-time applications. The real-time simulation model offers the benefits of testing different control algorithms along with hardware-in-the-loop testing. The bond graph-based dynamic modeling of a ship hybrid power system with a DC grid is presented as applicable to real-time simulation. The overall system model is established using different component models with varying fidelity, so-called mixed-modeling approach. In this approach, the components and control functions are modeled with different complexity such that it can capture the necessary system dynamics while minimizing the computational time. Results show that the modeled system is capable of simulating different operating strategies of the hybrid power system. Moreover, the mixed-modeling approach has enabled the system to simulate in nearly 2.5 times faster than the real-time.

I. INTRODUCTION

The maritime industry is adopting vessels with hybrid and electric power system to improve energy efficiency while complying with the stringent emission regulations [1], [2]. Electric propulsion with a combination of different energy carriers, as a feasible low-emission solution, is recently being widely adopted both in the newly built and retrofitted ships. It not only increases operational flexibility, reliability, redundancy, and safety but also helps to optimize the generator capacity, eventually minimizing average fuel consumption and emissions [3], which are reduced by 10-35% using a hybrid architecture and the advanced control strategies [4].

With the advancement of power systems in a vessel, complexities in the components and system level are increasing. While integrating new technologies, the modeling and simulation studies not only help in optimal operation but also during the design and maintenance phases [5]. The power system modeling is also required for its stability analysis [6], [7] along with performance evaluation for a system with nonlinear dynamics [8], [9]. Moreover, modeling of faults and abnormal conditions in the components and system levels is imperative for the design, testing, and training of such a complex system.

An energy-based bond graph modeling [10] offers the ease of interlinking physical subsystems in various domains through a power bond along with causality indication [11]. The modularity in the component level increases the efficiency of system model development. The modularity and system overview is well supported by its graphical representation. The easier extraction of the mathematical equations from the graph increases its application both in the stability and analytical studies. Moreover, model switching or variable routing through the use of switched power junctions [12] enhances its use for fault and failure modeling.

With the increase in the degree of fidelity in a model, its accuracy usually increases. However, it may decrease the computational efficiency. It is not always necessary to use a detailed model for each component while modeling a system. The choice of degree of fidelity depends on the objective of the simulation. Therefore, it is necessary to have models with varying complexities in the model library.

In this work, dynamic models for hybrid and electric components in a ship power system with DC grid are developed using bond graph modeling technique. The mixed-modeling approach is used for the integration of different component models with varying fidelity to develop an overall system model, which is able to capture the necessary system dynamics while minimizing the computational time. The system is able to simulate faster than real-time, making it applicable for real-time simulation.

This paper is structured into four sections. The system, along with component models, for a ship hybrid power system, are presented in section II. In section III, the simulation results for the system startup and load sharing strategies are included and analyzed. Finally, the work is concluded in section IV.

II. MODEL OF HYBRID POWER SYSTEM

DC power system is gaining more relevance in shipboard applications as it can easily be interfaced with energy storage devices (ESDs) [13]. Moreover, the variable speed operation of the diesel engine in the DC power system improves fuel efficiency and reduces emissions. A schematic of the implemented DC power system is shown in Fig. 1. The diesel engine generator set (genset) is connected to a DC bus through an

uncontrolled rectifier. The battery bank is connected to the DC bus through a bidirectional DC-DC converter. An induction motor, as a propulsion load, takes load torque as a reference. An inverter interfaces the load and the DC bus.
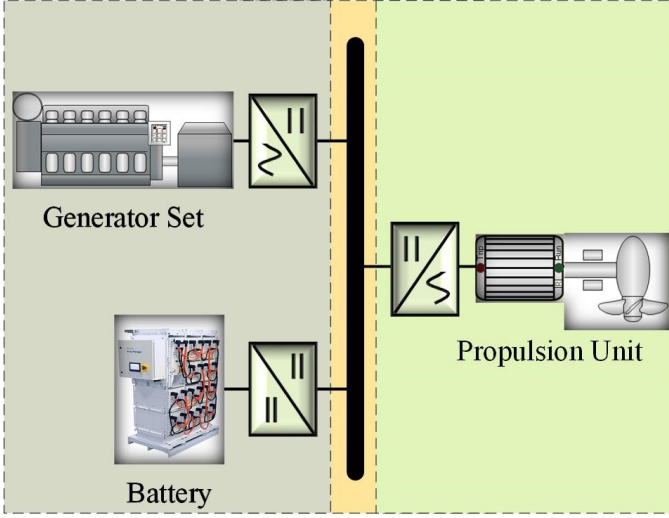

Fig. 1: Schematic of a shipboard DC hybrid power system.

A. Genset

The diesel engine is modeled as presented in [14]. The angular speed, displacement and mechanical torque is calculated as given in Eqn. (1)-(3).

$$\dot{\omega}_m = \frac{1}{J_m + J_G}(T_m - b_f\omega_m - b_b\omega_m^n - T_e) \tag{1}$$

$$\dot{\theta}_m = \omega_m \tag{2}$$

$$T_m = \frac{P_e}{\omega_m} = \frac{\dot{m}_f h_n \eta}{\omega_m} \tag{3}$$

J_m and J_G are the inertia of the engine and generator, respectively. T_e is the electromagnetic torque, b_f is a friction coefficient, b_b is a braking effect, n is typically 0.1. P_e is the effective engine power, h_n is the lower calorific heat value of the fuel, η is the engine efficiency and $\dot{m}_f$ is inlet fuel flow rate.

The two-axis-model of a synchronous generator is modeled based on [14]–[16],

$$\dot{\boldsymbol{\Psi}} = -\omega_m \boldsymbol{D}\boldsymbol{\Psi} - \boldsymbol{R}\boldsymbol{i} + \boldsymbol{E}\boldsymbol{u}_{d,q} + \boldsymbol{b}u_f \tag{4}$$

$$\boldsymbol{i} = \boldsymbol{L}^{-1}\boldsymbol{\Psi} \tag{5}$$

$$T_e = n_p(\psi_d i_q - \psi_q i_d) \tag{6}$$

where $\boldsymbol{\Psi} = [\Psi_d, \Psi_q, \Psi_f, \Psi_D, \Psi_Q]^T$ is the magnetic flux vector, $\boldsymbol{i} = [i_d, i_q, i_f, i_D, i_Q]^T$ is current vector, u_f is field voltage, n_p is number of generator pole pairs, $\boldsymbol{R}$ is resistance matrix, $\boldsymbol{L}$ is inductance matrix and $\boldsymbol{u}_{d,q}$ is voltage matrix. The synchronous generator model is then transformed to voltage-output model as presented in [14].

B. Propulsion Load

The propulsion load is modeled as an induction motor based on the two-reaction-theory [16]. The voltage balance equation for the induction motor in the dq-reference frame is written as in Eqn. (7)-(8), where $\boldsymbol{u}, \boldsymbol{i}, \boldsymbol{\psi}$ are voltage, current, and flux vectors, respectively. $\boldsymbol{R}, \boldsymbol{D}, \boldsymbol{L}$ are resistance, pole-pair and inductance matrices, respectively.

$$\boldsymbol{u} = \boldsymbol{R}\boldsymbol{i} + \frac{d\boldsymbol{\psi}}{dt} + \omega_m \boldsymbol{D}\boldsymbol{\psi} \tag{7}$$

$$\boldsymbol{i} = \boldsymbol{L}^{-1}\boldsymbol{\psi} \tag{8}$$

$$T_e = n_p(\psi_{ds}i_{qs} - \psi_{qs}i_{ds}) \tag{9}$$

$$\omega_m = \frac{1}{J}\int(T_e - T_L - T_f)dt \tag{10}$$

where, T_e, T_L, and T_f are electromagnetic, load and frictional torque, respectively. J is inertia and ω_m is mechanical speed.

C. Lithium-ion Battery

A simplified first-order electrical circuit model is implemented for modeling a lithium-ion battery bank [17], [18] (see Fig. 2), which is represented mathematically as given in Eqn. (11)-(15).

$$V_{oc} = V_{oc0} - K_e T(1 - SoC) \tag{11}$$

$$R_o = R_{o0}(1 + a_0(1 - SoC)) \tag{12}$$

$$R_1 = -R_{10}ln(1 - SoC) \tag{13}$$

$$C_1 = \frac{\tau_1}{R_1} \tag{14}$$

$$SoC = SoC_0 - \frac{1}{Q}\int_{t_0}^{t} I_{batt}dt \tag{15}$$

V_{oc} is the open-circuit voltage and R_o is the internal resistance of the battery. The set of parallel resistance (R_1) and capacitance (C_1) represents the battery dynamics. The state of charge is given by SoC. T is the temperature in kelvin (assumed constant), K_e and a_0 are battery constants. τ_1 is battery time constant, Q is battery capacity and I_{batt} is battery current. The electrochemical double layer phenomenon, diffusion phenomenon and ohmic losses are represented by C_1, R_1, and R_o, respectively.
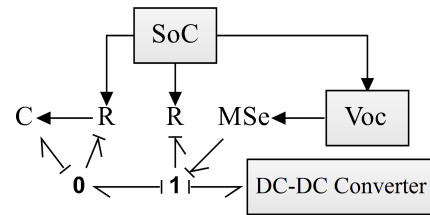

Fig. 2: Bond graph model of a battery.

The presented bond graph model for a lithium-ion battery is tested with the standard lithium-ion battery model in Simulink library [19]. An identical charge-discharge current waveform is applied to both the models and their voltage and SoC responses are presented in Fig. 3, which shows that SoC estimation in both the models are identical, whereas the voltage responses are similar with some deviations.
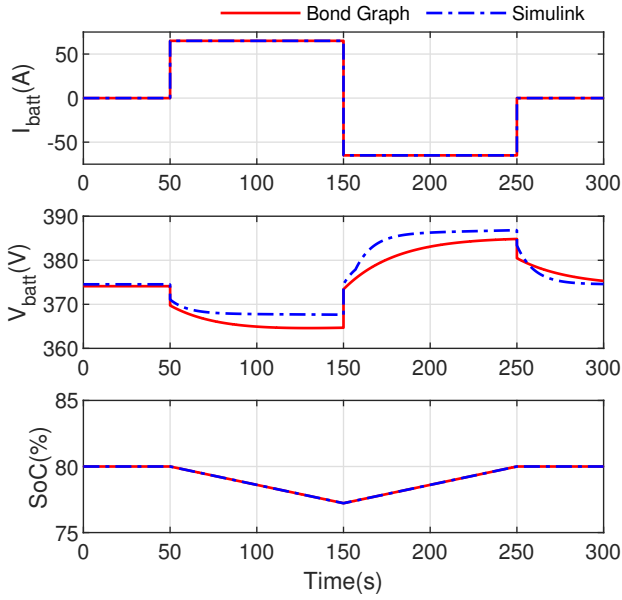
Fig. 3: Comparison of battery model responses.

Fig. 4: Uncontrolled three-phase rectifier model.

D. Uncontrolled Rectifier

An uncontrolled rectifier is used to interface the genset to the DC bus since the DC bus voltage can be regulated using the automatic voltage regulator (AVR) [5].

In the bond graph modeling technique, a **1**- and **0**-junction can only have one flow and effort deciding power bonds, respectively [10]. However, using the switched power junction represented as **1s** and **0s**, there can be two or more flow or effort deciding power bonds for **1s** and **0s**, respectively. A constraint is implemented in such a junction to choose only one flow or effort deciding power bonds, respectively for **1s** and **0s** at the mutually exclusive time instants [12].

1) Switched Model: A three-phase diode bridge rectifier is modeled using switched-mode power junctions (see Fig. 4). The forward biased diodes are selected by the logic implemented in '<' and '>'.

2) Average Model: An average rectifier is modeled in dq reference frame based on [15],

$$U_{LL} = \sqrt{\frac{2}{3}}\sqrt{u_d^2 + u_q^2} \tag{16}$$

$$I_{DC} = \frac{\pi}{3\omega L_s}(\frac{3\sqrt{2}}{\pi}U_{LL} - U_{DC}) \tag{17}$$

$$i_d = \frac{1}{u_d^2 + u_q^2}(u_d P + u_q Q) \tag{18}$$

$$i_q = \frac{1}{u_d^2 + u_q^2}(u_q P - u_d Q) \tag{19}$$

U_{LL} is rms line-to-line voltage, ω is the angular frequency of the generator, Ls is generator side inductance, I_{DC} is the average DC current. P and Q are active and reactive power. i_d, u_d, i_q, and u_q are current and voltage in d- and q-axes, respectively.
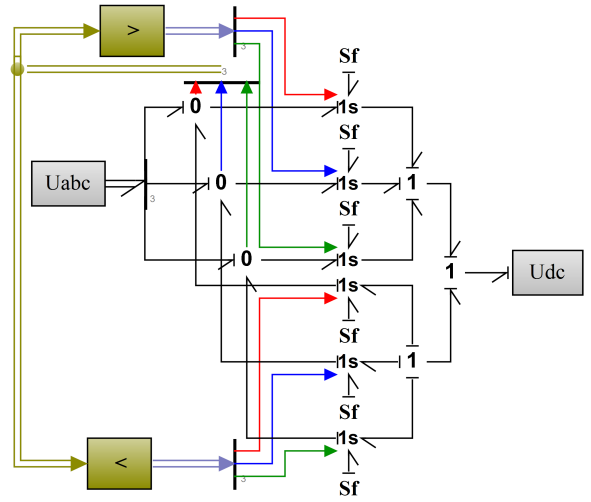
E. Bidirectional DC-DC Converter

The bond graph model of a bidirectional DC-DC converter is developed using switched-mode power junctions (see Fig. 5), which is analogous to the non-inverted buck-boost converter [20] (see Fig. 6). Switching signals for buck and boost switches along with the operating mode (boost or buck) are inputs to the model. **1s** represents the switch with anti-parallel diode, whereas **0s** represents switching between the buck or boost switches.
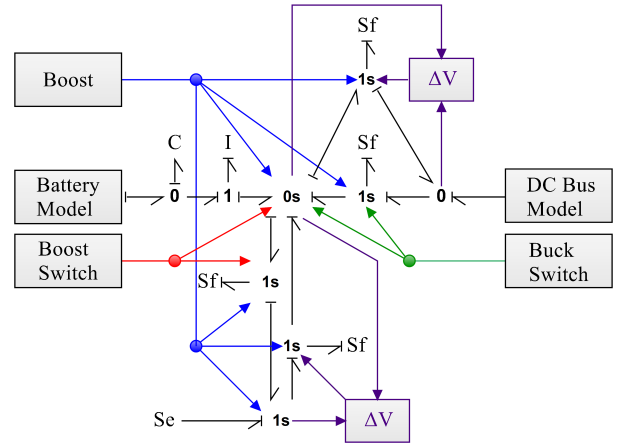

Fig. 5: A non-inverted buck-boost converter model implemented in the bond graph.

The DC-DC converter switching is regulated to operate the converter both in charging and discharging modes. The cascaded power-current controller, followed by pulse width modulation, is implemented to achieve the demanded power transfer between the battery and constant voltage (565 V) DC bus. The discharge-charge power waveform with an amplitude of 30 kW is applied to both the DC-DC converters in Fig. 5-6, and the results are compared in Fig. 7.
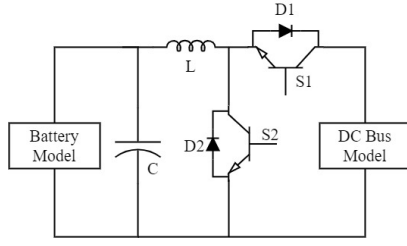
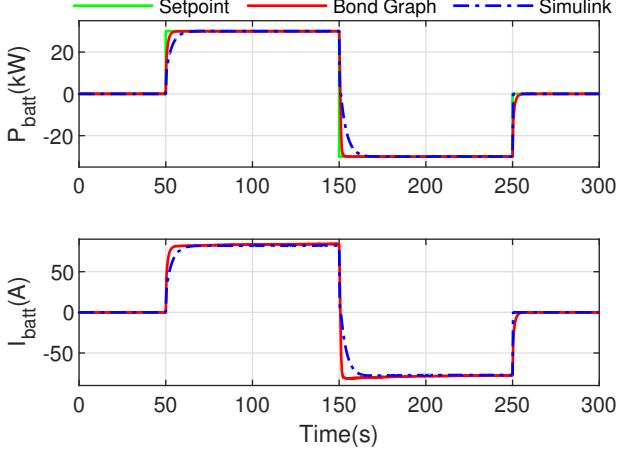Fig. 6: A non-inverted buck-boost converter model implemented in Simulink.

Fig. 7: Comparison of voltage and power responses.

F. Voltage Source Inverter (VSI)

1) Switched Model: The VSI is modeled using switched-mode power junctions (see Fig. 8). The DC voltage is branched into six power bonds from **0**-junction, where the currents are added. Transformers (TF) are used to invert the voltage and current. Based on the switching signals generated by PWM, **1s** selects either of the inputs. Voltages from two **1s**'s are combined at **1**-junction to generate a phase voltage.
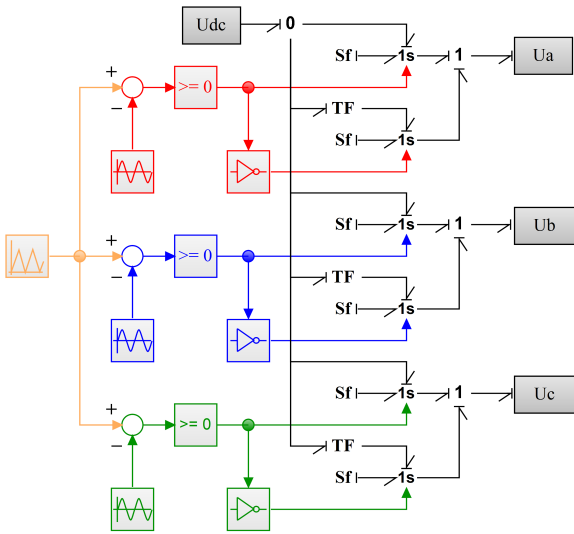

Fig. 8: Three-phase inverter model.

2) Average Model: The average model of a PWM VSI in the d-q reference frame is implemented using modified transformer (MTF) in bond graph methodology based on [5],

$$\begin{bmatrix} u_q \\ u_d \end{bmatrix} = m \begin{bmatrix} sin(\phi_0 - \theta) \\ cos(\phi_0 - \theta) \end{bmatrix} U_{DC} \tag{20}$$

$$I_{DC} = m(i_q sin(\phi_0 - \theta) + i_d cos(\phi_0 - \theta)) \tag{21}$$

where m is the modulation index, ϕ_0 is an initial arbitrary phase angle and θ is the d-q transformation angle.

III. SIMULATION RESULTS AND DISCUSSION

The mixed-modeling approach, a combination of component models with different degrees of fidelity, is used to select the converter models. In this system simulation, a power-based rectifier model (Eqn. 16 - 19), an ideal switch-based bidirectional DC-DC converter (Fig. 5 (b)) and an average inverter model (Eqn. 20 - 21) are used. This concept of mixed-modeling is used to reduce computational time. The simulation period of 30 s is simulated in approximately 12 s, which enhances the possibility of running the system simulation in real-time. Moreover, the effectiveness of the model under different operating conditions are demonstrated through the simulation results. In a load sharing control approach between the generator and the battery, different operating modes are to be considered, as simulated and presented in this section. Table I depicts the simulation parameters.

TABLE I: Simulation parameters.

Genset	400 kVA, 1200 - 1800 rpm, 440 Vrms
DC bus	565 V
Battery	Li-ion, 65 Ah, 346 V
Induction Motor	160 kW at 1500 rpm
DC-DC Converter	2 kHz, 100 mH, 300 μF
Step Size (time)	30 μs
Simulated Duration	30 s
Computational Time	approx. 12 s

A. System Startup

To study the dynamics of the system, the hybrid power system startup is simulated for 30 s. The events in this simulation are depicted in Table II and the system responses are included in Fig. 9 and 10. While starting the induction motor at 7 s, peaks in voltage and power curves are observed due to high starting torque of the motor. When a load torque of 1000 Nm is applied to the motor at 10s, both the generator and the battery supply the load (in this case in a fixed ratio). It can also be observed that the engine has variable speed (based on the load power) as the system frequency need not be maintained for the DC bus. The propulsion motor speed is also controllable through a drive.

TABLE II: Simulation events.

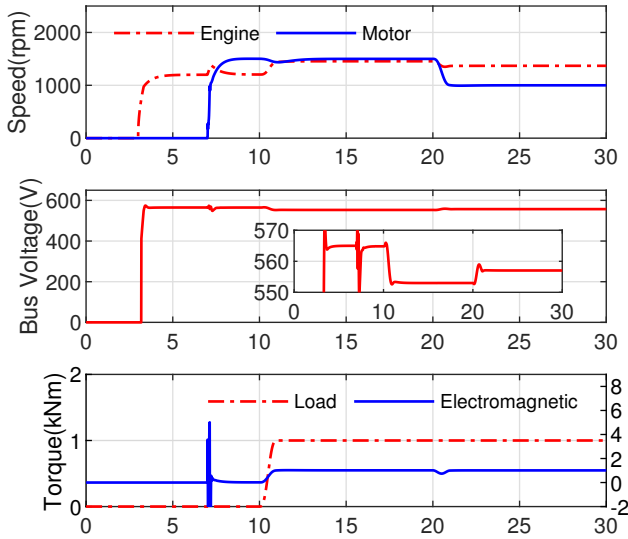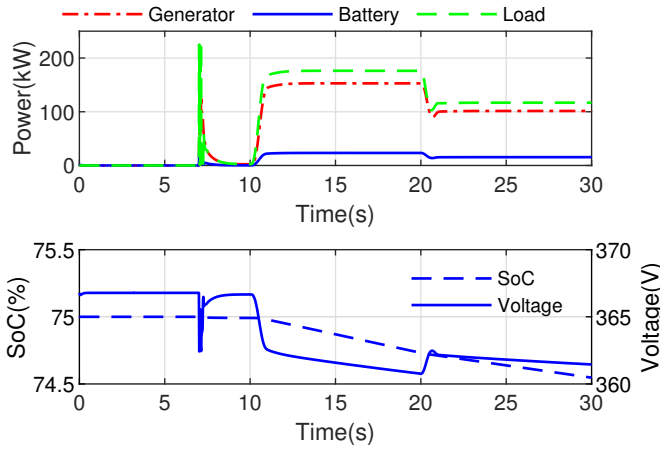| Time	Events
3 s	Engine started, and bus energized
7 s	Load bus connected and the motor started
10 s	1000 Nm Load torque applied to the motor
20 s	Motor speed decreased to 1000 rpm

Fig. 9: System startup simulation responses.

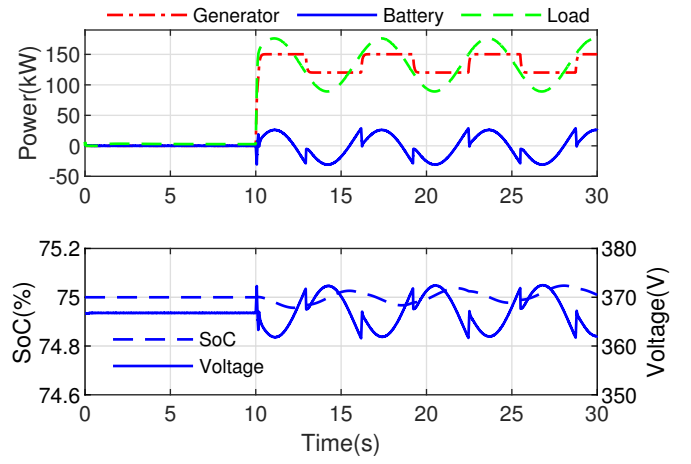Fig. 10: Load sharing after system startup.

Fig. 11: Load sharing through peak shaving strategy.

or discharge depending on the load variations (see Fig. 12), thereby limiting unnecessary generator power fluctuation.
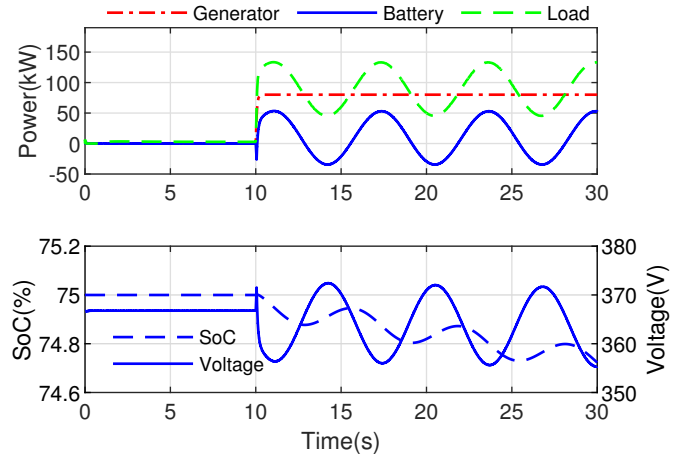

Fig. 12: Load sharing through load leveling strategy.

B. Load-sharing strategies

There are various strategies for the optimal use of ESDs in a ship hybrid power system [21], such as peak shaving, zero-emission operation, battery charging, enhanced dynamic performance, spinning reserve, and strategic loading. Different simulation cases are developed to simulate some of those strategies. For further simulations, the system is initially energized with the generator, motor, and battery in running state. The load torque and motor speed change are applied to observe the dynamics of the system for different load sharing strategies.

1) Peak Shaving: In peak shaving, battery will either charge or discharge depending on the loading condition, while ensuring that the generator operates between predefined load limits (see Fig. 11). It inhibits the unnecessary load dependent start-stop of the engine due to fluctuating nature of shiploads.

2) Load Leveling: In load leveling, the generator is supplying average load power while the battery will either charge

3) Zero-Emission: During the zero-emission operation, battery supplies the total load demand (see Fig. 13). In general, a battery bank power capacity in a hybrid ship is lower than the conventional engine. The battery bank and the converter should be designed to supply the required power to the propulsion system, and critical auxiliaries to enable zero-emission operation. The battery bank can either supply higher loads for a shorter time or vice versa. Therefore, proper planning for zero-emission operation is critical to make sure that the battery SoC is within the limits. In this simulation case, the load torque setpoint is decreased to 250 Nm to match the capacity of the battery.

4) Battery Charging: Before a zero-emission operation mode, the battery needs to be fully charged. Battery charging onboard is simulated (see Fig. 14), where the generator is supplying power not only to recharge the battery but also to operate the propulsion load.
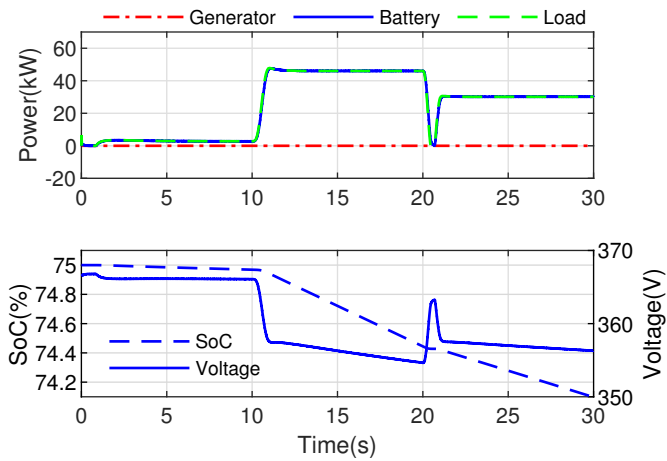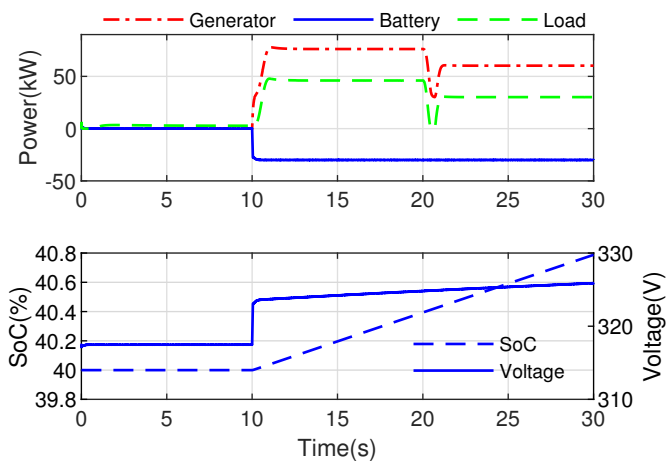
Fig. 13: Zero-emission operation.

Fig. 14: Battery charging operation.

IV. Conclusion

In this work, a bond graph-based shipboard DC hybrid power system has been modeled using the mixed-modeling approach. The mixed-modeling approach reduced the complexity of the system model. It also enabled the system model to simulate approximately 2.5 times faster than the real-time. Moreover, the simulation results show that the model is able to capture the required system dynamics for different strategic operations of battery in the ship hybrid power system. This unified simulation framework is further applicable for dynamic analysis of the hybrid power system.

Acknowledgment

References

[1] P. Ghimire, D. Park, M. K. M. Zadeh, J. Thorstensen, and E. Pedersen, "Shipboard Electric Power Conversion: System Architecture, Applications, Control, and Challenges [Technology Leaders]," *IEEE Electrification Magazine*, vol. 7, no. 4, pp. 6–20, Dec. 2019.

[2] M. B. Othman, N. P. Reddy, P. Ghimire, M. K. Zadeh, A. Anvari-Moghaddam, and J. M. Guerrero, "A Hybrid Power System Laboratory: Testing Electric and Hybrid Propulsion," *IEEE Electrification Magazine*, vol. 7, no. 4, pp. 89–97, Dec. 2019.

[3] ABS, "ABS Advisory on Hybrid Electric Power Systems," American Bureau of Shipping, Tech. Rep., 2017.

[4] R. D. Geertsma, R. R. Negenborn, K. Visser, and J. J. Hopman, "Design and control of hybrid power and propulsion systems for smart ships: A review of developments," *Applied Energy*, vol. 194, pp. 30–54, May. 2017.

[5] B. Zahedi and L. E. Norum, "Modeling and Simulation of All-Electric Ships With Low-Voltage DC Hybrid Power System," *IEEE Transactions on Power Electronics*, vol. 28, no. 10, pp. 4525–4537, Oct. 2013.

[6] D. Park and M. K. Zadeh, "Dynamic Modeling and Stability Analysis of Onboard DC Power System for Hybrid Electric Ships," in *ITEC 2019 - 2019 IEEE Transportation Electrification Conference and Expo*, Institute of Electrical and Electronics Engineers Inc., Jun. 2019.

[7] M. K. Zadeh, R. Gavagsaz-Ghoachani, B. Nahid-Mobarakeh, S. Pierfederici, and M. Molinas, "Stability analysis of hybrid AC/DC power systems for more electric aircraft," in *Conference Proceedings - IEEE Applied Power Electronics Conference and Exposition - APEC*, vol. 2016-May, pp. 446–452. Institute of Electrical and Electronics Engineers Inc., May. 2016.

[8] M. K. Zadeh, R. Gavagsaz-Ghoachani, S. Pierfederici, B. Nahid-Mobarakeh, and M. Molinas, "Stability Analysis and Dynamic Performance Evaluation of a Power Electronics-Based DC Distribution System with Active Stabilizer," *IEEE Journal of Emerging and Selected Topics in Power Electronics*, vol. 4, no. 1, pp. 93–102, Mar. 2016.

[9] M. K. Zadeh, R. Gavagsaz-Ghoachani, J. P. Martin, S. Pierfederici, B. Nahid-Mobarakeh, and M. Molinas, "Discrete-Time Tool for Stability Analysis of DC Power Electronics-Based Cascaded Systems," *IEEE Transactions on Power Electronics*, vol. 32, no. 1, pp. 652–667, Jan. 2017.

[10] D. Karnopp, D. L. Margolis, and R. C. Rosenberg, *System dynamics : modeling, simulation, and control of mechatronic systems*. Wiley, 2012.

[11] P. C. Breedveld, "Port-based modeling of mechatronic systems," *Mathematics and Computers in Simulation*, vol. 66, no. 2-3, pp. 99–128, Jun. 2004.

[12] A. C. Umarikar and L. Umanand, "Modelling of switching systems in bond graphs using the concept of switched power junctions," *Journal of the Franklin Institute*, vol. 342, no. 2, pp. 131–147, 2005.

[13] R. S. Balog and P. T. Krein, "Bus selection in multibus DC microgrids," *IEEE Transactions on Power Electronics*, vol. 26, no. 3, pp. 860–867, 2011.

[14] S. Skjong and E. Pedersen, "A real-time simulator framework for marine power plants with weak power grids," *Mechatronics*, vol. 47, pp. 24–36, Nov. 2017.

[15] T. A. Pedersen and E. Pedersen, "Bond graph modelling of marine power systems," *Mathematical and Computer Modelling of Dynamical Systems*, vol. 18, no. 2, pp. 153–173, 2012.

[16] D. Sahm, "A two-axis, bond graph model of the dynamics of synchronous electrical machines," *Journal of the Franklin Institute*, vol. 308, no. 3, pp. 205–218, 1979.

[17] K. Benabdelaziz and M. Maaroufi, "Battery dynamic energy model for use in electric vehicle simulation," *International Journal of Hydrogen Energy*, vol. 42, no. 30, pp. 19 496–19 503, Jul. 2017.

[18] L. I. Silva, J. Jaguemont, C. H. De Angelo, and L. Boulon, "Modeling an Electric Vehicle Lithium-Ion Battery Pack Considering Low Temperature Behavior," in *2016 IEEE Vehicle Power and Propulsion Conference (VPPC)*, pp. 1–5. IEEE, Oct. 2016.

[19] The MathWorks Nordic, "Generic battery model - Simulink."

[20] M. S. Saleh, A. Althaibani, Y. Esa, Y. Mhandi, and A. A. Mohamed, "Impact of clustering microgrids on their stability and resilience during blackouts," in *2015 International Conference on Smart Grid and Clean Energy Technologies (ICSGCE)*, pp. 195–200. IEEE, Oct. 2015.

[21] A. J. Sorensen, R. Skjetne, T. Bo, M. R. Miyazaki, T. A. Johansen, I. B. Utne, and E. Pedersen, "Toward Safer, Smarter, and Greener Ships: Using Hybrid Marine Power Plants," *IEEE Electrification Magazine*, vol. 5, no. 3, pp. 68–73, Sep. 2017.